Design and Testing of Small-Scale Unsteady-State Afterburners and Reactors

Davide Fissore, Antonello A. Barresi, and Giancarlo Baldi
Dipartimento di Scienza dei Materiali ed Ingegneria Chimica, Politecnico di Torino, 10129 Torino, Italy

Miguel A. G. Hevia, Salvador Ordóñez, and Fernando V. Díez
Departamento de Ingeniería Química y Tecnología del Medio Ambiente, Universidad de Oviedo, 33006 Oviedo, Spain

DOI 10.1002/aic.10430
Published online April 13, 2005 in Wiley InterScience (www.interscience.wiley.com).

The design and testing of small-scale and pilot-scale apparatus using the reverse-flow concept is focused on. The combustion of lean air–methane mixtures was considered as a test reaction both for modeling purposes and for the experimental investigation. A one-dimensional two-phase model was used to highlight that thermal properties of the reactor wall and radial heat losses affect the thermal stability of bench-scale rigs more than that of large-scale industrial reactors, where adiabatic behavior is generally achieved. As a consequence, a special temperature-control system, based on dynamic compensation of the thermal losses, was designed to attain adiabatic operation in a small-scale apparatus, avoiding overcompensation and thus allowing the scale-up of the results obtained. This system was realized and tested, proving to be effective in a wide range of operating conditions such as inlet concentration and feed flow rate. © 2005 American Institute of Chemical Engineers *AIChE J,* 51: 1654–1664, 2005
Keywords: reverse-flow reactor, autothermal combustion, temperature control, adiabatic reactor, bench-scale reactor

Introduction

The results obtained by experimental investigation in bench-scale reactors may be substantially affected not only by the operating conditions but also by wall effects: because of the wall thermal conductivity and the ratio between reactor surface and volume, it is particularly difficult to obtain adiabatic conditions that are generally achieved in an industrial-scale apparatus. This poses a number of problems in the scale-down of industrial-size reactors, and may produce unreliable results in pilot-scale demonstration units. For example, an inlet pollutant concentration that allows for autothermal operation in an industrial-size *reverse-flow reactor* (RFR) may lead to reaction extinction in a laboratory-scale rig because of the wall heat losses. As a consequence, results obtained in a lab-scale reactor cannot be used to design an industrial apparatus. Moreover, RFR is a challenging case study because the operating conditions are particularly severe: in every point of the reactor the temperature and the concentration exhibit oscillating values and the reactor never operates in a steady state.

The RFR was thoroughly investigated in the past because the reversal of the flow direction gives rise to special temperature profiles. These profiles can improve the yield in exothermal equilibrium limited reactions and, in the case of afterburners, they can allow autothermal operation, even when cold and lean mixtures are fed. The reversal of the flow keeps the heat of reaction inside the bed, thus reducing (or even eliminating) the need for auxiliary fuel, except for the start-up and for control purposes. After the transient period after the start-up, a *pseudo-steady state* (PSS), also called cyclic steady state, is attained in

Correspondence concerning this article should be addressed to A. A. Barresi at antonello.barresi@polito.it.

the RFR: the hot front shifts periodically in the central part of the reactor, whereas the ending parts of the bed remain cold, allowing a very low heat loss in the outlet flow. For this reason, the catalyst, in the external parts of the bed, can be substituted by inert material. Extensive investigations about the RFR, including both numerical simulations and experimental analysis, were performed in the past 30 years and were reviewed, for example, in Matros and Bunimovich.[1]

Fissore and Barresi[2] reported that performance of the RFR strongly depends on the physical properties of the packing (catalyst and inert), that is, density, specific heat, and thermal conductivity. As a result, the thermal efficiency of the RFR is closely related to the capability of keeping the heat of reaction in the central part of the bed, whereas the sides work as heat exchangers; as a consequence, the lower the axial heat dispersion (in the gas phase) and axial heat conduction (in the solid phase), the higher the thermal efficiency. Less attention was paid to the influence of the reactor wall on the performance of the system[3]: reactor walls are usually made from metals, whose high thermal conductivity and heat capacity may strongly contribute to the thermal balance of the system, particularly if the reactor size is small. The results obtained by an experimental investigation in a bench-scale rig can thus cause deviations in the prediction of the performance of an industrial reactor. That is why wall effects must be taken into account both in the design and in the evaluation of results obtained in lab- or bench-scale reactors and a system devoted to compensating the heat losses must be designed in lab-scale rigs to allow for the scale-up.

Different technical solutions were proposed in the past to confront this problem: standard insulation,[4] evacuated jacket,[5] or steady electrical thermal compensation. Nieken et al.[6] and Eigenberger and Nieken[7] used a reactor insulated with a layer of mineral fiber with an electrical heater placed in the central part. To avoid overcompensation, the temperature of the heater was controlled to a value about 20 K below the value measured in the central axial position of the catalyst. A reasonable but not perfect compensation of heat losses was achieved: a shallow dent in the middle of the temperature profile was not avoided. Zufle and Turek[8] provided the reactor with a homogeneous electrical heating on the wall to maintain adiabatic operation. Nevertheless, this method does not allow one to attain a real adiabatic configuration: the solid temperature changes quickly in time and space from 20 to 500–600°C, so that a homogeneous steady heating can completely stop the cooling of the hot zones and, at the same time, it can actively heat the cold zones. Even if the two heat flows compensate each other and the reactor is virtually adiabatic in the average, the global effect is a bypass of heat from the hot central part of the reactor to the cold ends, with a decrease in the thermal efficiency.

To avoid these problems, we used a different approach: the adiabatic behavior is simulated by means of a special temperature-control system based on a dynamic compensation of the thermal losses. The reactor wall is surrounded by a number of independent band heaters, whose temperatures are controlled by independent relays, so that each one constantly keeps the same temperature of the part of the reactor that directly faces that heater. The dynamic behavior of the reactor has the problem such that the temperature in each point of the reactor is not constant, but changes during the operation, and may either increase or decrease. As a consequence, not only must a heating device be provided, but also a cooling system is also needed to follow the dynamics of the temperature inside the reactor when it is decreasing. Moreover, the dynamics of the heating/cooling system has to be faster than that of the reactor to avoid interferences with the thermal balance of the system.

The treatment of the lean fugitive emissions from coke ovens was investigated in this rig, in the framework of a European Project (ENV4-CT97-0599). The composition of these mixtures may be very complex and variable with time according to the operation, such as charging, pushing, and door leaks. Pushing emissions are composed of humid air with about 5% carbon dioxide and 200 ppmV carbon monoxide. Composition of charging and door emissions is similar but, taking into account the volume emitted, the most dangerous emissions are those produced during the charging of the coke ovens: methane is present in relatively high concentration; H_2O, H_2S, SO_2, and other compounds are also present in a lower concentration. Methane is also very adequate as a test compound for catalytic destruction studies because, for a well-defined catalyst composition, it has the highest ignition temperature among paraffinic and aromatic compounds and, as a consequence, most pollutants will be destroyed at the temperature that allows for total methane combustion. Moreover, the GWP (global warming potential) of methane is about 20 times higher than that of carbon dioxide, which forms from methane combustion, and thus its transformation to carbon dioxide is environmentally advantageous.

The Model

A one-dimensional heterogeneous model was used to investigate the influence of the main operating parameters on the stability of the RFR; justification for neglecting radial temperature gradients was that the radial Biot number is very small, even though radial heat transport is significant. Pressure loss inside the system was neglected and plug flow, with dispersive transport of mass and energy, was assumed for the gas phase; the ideal gas law was used. The transient term was taken into account in the gas-phase equations and in the energy equation for the solid phase, whereas the solid catalytic surface was considered in the pseudo-steady-state condition. The effect of the intraparticle mass transport was included in the model by means of the effectiveness factor. Thus, the dynamics of the adiabatic process can be described by the following set of partial differential-algebraic equations (PDAEs).

Continuity Equation for the Gas Phase

$$\frac{\partial c_G}{\partial t} + \frac{\partial}{\partial x} c_G v = \sum_{i=1}^{n_r} \frac{k_{G,i} a_v}{\varepsilon} (y_{S,i} - y_{G,i}) \tag{1}$$

Continuity Equation for Component j in the Gas Phase

$$\frac{\partial y_{G,j}}{\partial t} = D_{eff} \frac{\partial^2 y_{G,j}}{\partial x^2} - v \frac{\partial y_{G,j}}{\partial x} + \frac{k_{G,j} a_v}{c_G \varepsilon} (y_{S,j} - y_{G,j}) - y_{G,j} \sum_{i=1}^{n_r} \frac{k_{G,i} a_v}{c_G \varepsilon} (y_{S,i} - y_{G,i}) \tag{2}$$

where $j = 1 \cdots (n_r - 1)$.

Energy Balance for the Gas Phase

$$\frac{\partial T_G}{\partial t} = \frac{k_{eff}}{\rho_G c_{p,G}} \frac{\partial^2 T_G}{\partial x^2} - v \frac{\partial T_G}{\partial x} + \frac{h a_v}{\rho_G c_{p,G} \varepsilon} (T_S - T_G) \tag{3}$$

Mass Balance for the Solid Phase

$$k_{G,j} a_v (y_{S,j} - y_{G,j}) = [\rho_S (1 - \varepsilon)] \sum_{k=1}^{N_R} \eta_k \nu_{j,k} R'_{k,j} \qquad j = 1 \cdots n_r \tag{4}$$

Energy Balance for the Solid Phase

$$\frac{\partial T_S}{\partial t} = \frac{\lambda_S}{\rho_S c_{p,S}} \frac{\partial^2 T_S}{\partial x^2} - \frac{h a_v}{\rho_S c_{p,S} (1 - \varepsilon)} (T_S - T_G) + \frac{1}{c_{p,S}} \sum_{i=1}^{n_r} \left(\sum_{k=1}^{N_R} \eta_k \nu_{i,k} R'_k \right) (-\Delta H_{f,i}) \tag{5}$$

For the catalytic part of the reactor, a first-order rate equation was considered in the mass balance

$$R'_{k,j} = k_r y_{S,j} = k_\infty \exp(-E_a / R T_S) y_{S,j} \tag{6}$$

$$k_\infty = k'_\infty \rho_S (1 - \varepsilon) R T_G \tag{7}$$

whereas for the inert sections the reaction rate was set equal to zero. Similarly, the solid physical properties, that is, density, specific heat, and thermal conductivity, were set equal to the values either of the catalyst or of the inert, depending on the axial position in the reactor. If the physical and transport properties of the catalyst and of the inert are different, adequate boundary conditions (that is, identity in the heat and mass fluxes) must be specified at the boundary surface.

When small-scale apparatuses are considered, a further equation is required to take into account the effect of the reactor wall on the thermal balance of the system (in our experimental equipment, for instance, the wall heat capacity amounts to about 30% of the whole system)[3]

$$\frac{\partial T_W}{\partial t} = \frac{\lambda_W}{c_{p,W} \rho_W} \frac{\partial^2 T_W}{\partial x^2} + \frac{4}{c_{p,W} \rho_W (D_{R,e}^2 - D_{R,i}^2)} D_{R,i} h_i (T_G - T_W) \tag{8}$$

and the energy balance for the gas phase is modified accordingly

$$\frac{\partial T_G}{\partial t} = \frac{k_{eff}}{\rho_G c_{p,G}} \frac{\partial^2 T_G}{\partial x^2} - v \frac{\partial T_G}{\partial x} + \frac{h a_v (T_S - T_G)}{\rho_G c_{p,G} \varepsilon} - \frac{4 h_i}{\rho_G c_{p,G} D_{R,i}} (T_G - T_W) \tag{9}$$

Conventional Danckwerts boundary conditions were assumed in $x = 0$ and $x = L$. Initially, the gas-phase temperature was considered constant along the reactors and equal to the inlet value, and the solid temperature was considered constant and equal to the preheating value.

Transport and dispersion parameters were evaluated according to previous works on the same subject.[9] Concerning the gas–solid heat transfer coefficient, the following correlation was adopted

$$\frac{h d_P}{\lambda_G} = 1.6 (2 + F \cdot \mathrm{Re}_P^{0.5} \mathrm{Pr}^{1/3}) \tag{10}$$

with

$$F = 0.664 \sqrt{1 + \left[\frac{0.0557 \cdot \mathrm{Re}_P^{0.3} \mathrm{Pr}^{2/3}}{1 + 2.44 (\mathrm{Pr}^{2/3} - 1) \mathrm{Re}_P^{-0.1}} \right]^2} \tag{11}$$

and a similar correlation was used to evaluate the mass transfer coefficient, according to Chilton–Colburn's analogy. The prediction of the gas axial heat dispersion coefficient was carried out by adopting a correlation by Dixon and Cresswell[10]

$$\frac{k_{eff}}{\rho_G v c_{p,G} d_P} = \frac{0.73 + \lambda_{st} / \lambda_G}{\mathrm{Re}_P \mathrm{Pr}} + \frac{0.5}{1 + 9.7 / (\mathrm{Re}_P \mathrm{Pr})} \tag{12}$$

According to Edwards and Richardson[11] a correlation of the same form was used for the prediction of mass dispersion:

$$\frac{D_{eff}}{v_G d_P} = \frac{0.73}{\mathrm{Re}_P \mathrm{Sc}} + \frac{0.5}{1 + 9.7 / (\mathrm{Re}_P \mathrm{Sc})} \tag{13}$$

The influence of the temperature and composition on the density and on the specific heat of the gas was taken into account.

When nonadiabatic operation is considered, a term accounting for the heat transport from the reactor wall to the surroundings is required in the wall thermal balance

$$\frac{\partial T_W}{\partial t} = \frac{\lambda_W}{c_{p,W} \rho_W} \frac{\partial^2 T_W}{\partial x^2} + \frac{4}{c_{p,W} \rho_W (D_{R,e}^2 - D_{R,i}^2)} D_{R,i} h_i (T_G - T_W) + \frac{h_w 4 D_{R,e} L}{c_{p,W} \rho_W} (T_W - T_e) \tag{14}$$

Also when the role of the wall is neglected, the term accounting for heat transfer to the surroundings must be added to the gas-phase energy balance (Eq. 3), which is thus modified to

$$\frac{\partial T_G}{\partial t} = \frac{k_{eff}}{\rho_G c_{p,G}} \frac{\partial^2 T_G}{\partial x^2} - v \frac{\partial T_G}{\partial x} + \frac{h a_v}{\rho_G c_{p,G} \varepsilon} (T_S - T_G) + \frac{h_w \pi D_{R,e} L}{\rho_G c_{p,G} \varepsilon} (T_G - T_e) \tag{15}$$

The domain of the spatial variable x was discretized on a grid of equally spaced points; 101 points are sufficient to ensure a

Table 1. Main Operating Parameters Considered in the Simulations of the RFR

Preheating temperature	673 K
Pellet diameter	3–5 mm
Catalyst density, ρ_S	1541 kg m^{-3}
Catalyst specific heat, $c_{p,S}$	836 J kg^{-1} K^{-1}
Catalyst porosity	0.451
Catalyst tortuosity	2
Catalyst thermal conductivity, λ_{eff}	0.042 W m^{-1} K^{-1}
Bed void fraction, ε	0.36
Frequency factor, k'_∞	774.3 mol kg^{-1} s^{-1} Pa^{-1}
Activation energy, E_{att}	1.223 $\times$ 10^5 J mol^{-1}
Inlet gas temperature	303 K

grid-independent solution. As a consequence, the PDAE system (Eqs. 1–5) was transformed into a differential algebraic equation (DAE) problem. The integration in time of the differential part of the system was performed by implementing the Fortran routine LSODES, from the package ODEPACK.[12] Both relative and absolute tolerance were set to the square root of the working machine precision.

After a transient period, the solution of the system evolves toward a pseudo-steady state (PSS), given that the behavior of the reactor (temperature and concentration profiles) is the same within every cycle.

Design Guidelines from Modeling

The main concern in the design of a bench-scale reactor is obtaining the proper operating conditions to achieve the same behavior of a large-scale industrial reactor to allow for the scale-up of the results. The effect of reactor size on the performance of the reactor was investigated by means of numerical simulations and the main parameters are shown in Table 1. Figure 1 shows the comparison between the solid temperature profiles obtained when the nonadiabatic operation is simulated in a reactor of different size; wall thermal balance is not

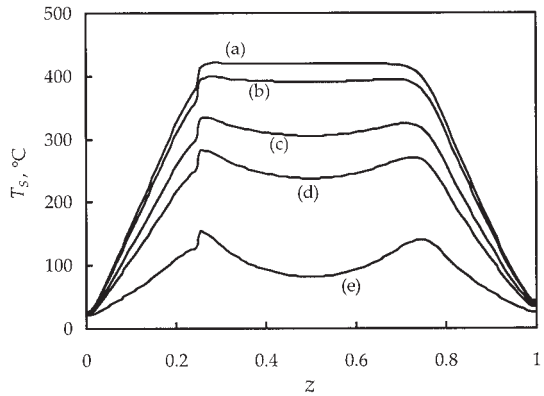

Figure 1. Comparison between the solid temperature profiles in an adiabatic reactor and when nonadiabatic conditions are considered (h_W = 0.18 W m^{-2} K^{-1}).

The profiles are taken in the middle of a semiperiod when the PSS is reached (t_c = 300 s, $y_{CH_{4,0}}$ = 1000 ppmV, $u_{G,0}$ = 0.1 m s^{-1}). Curve (a): adiabatic reactor; curve (b): D_R = 0.5 m; curve (c): D_R = 0.1 m; curve (d): D_R = 0.05 m; curve (e): D_R = 0.01 m.

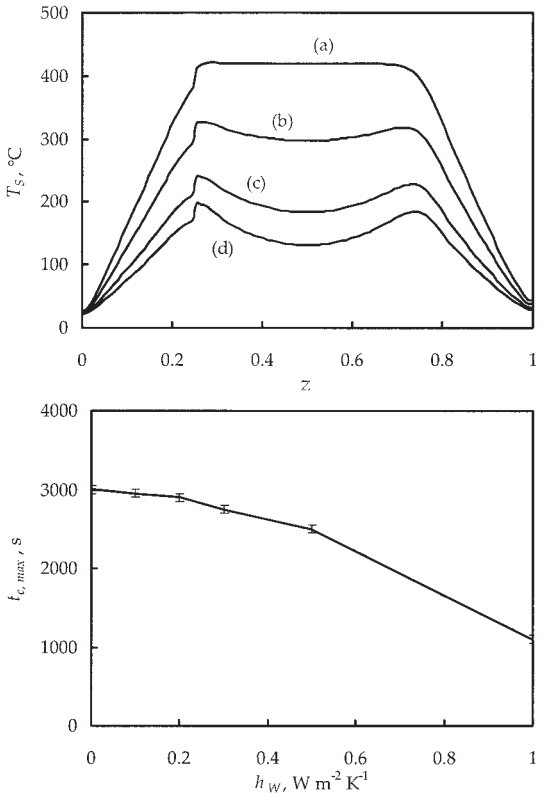

Figure 2. Comparison between the solid temperature profiles in a nonadiabatic reactor (top graph, t_c = 300 s; the profiles are taken in the middle of a semiperiod when the PSS is reached) and maximum switching time that allows stable autothermal combustion (bottom graph) for various values of the heat transfer coefficient between the reactor and the environment.

$D_{R,e}$ = 0.05 m^{-1}, wall thickness: 2 mm, $y_{CH_{4,0}}$ = 1000 ppmV, $u_{G,0}$ = 0.1 m s^{-1}. Curve (a): adiabatic reactor; curve (b): h_W = 0.1 W m^{-2} K^{-1}; curve (c): h_W = 0.3 W m^{-2} K^{-1}; curve (d): h_W = 0.5 W m^{-2} K^{-1}.

considered. It is evident that for large-scale reactors adiabatic behavior may be assumed, whereas in small-scale reactors heat losses strongly affect the temperature profiles and thus the thermal stability of the system. This is a consequence of the dependency of the thermal efficiency on the ratio between the reactor surface and the reactor volume, and therefore on the reactor diameter.

The higher the heat exchange coefficient from the solid to the surroundings, the higher the effect of heat losses on the temperature profiles, as shown in Figure 2, where the influence of the heat-exchange coefficient on the maximum switching time that allows for autothermal behavior is also shown. As a consequence the influence of nonadiabaticity on the results obtained in a bench-scale rig (thus in a nonadiabatic system) has to be taken into account to allow for a correct scale-up to an industrial reactor (thus an adiabatic system): the inlet pollutant concentration that allows for autothermal operation in an industrial-size RFR can in fact lead to reaction extinction in a lab-scale rig because of the wall heat losses. Also the value of

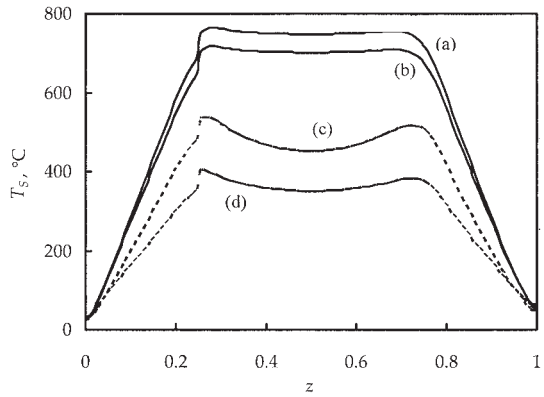

Figure 3. Comparison between the solid temperature profiles in a nonadiabatic reactor (h_W = 0.18 W m^{-2} K^{-1}) when the thermal balance of the quartz wall is considered or neglected.

Curve (a) $D_{R,e}$ = *0.5 m, without wall thermal balance; curve (b)* $D_{R,e}$ = 0.5 m, with wall thermal balance; curve (c) $D_{R,e}$ = 0.05 m, without wall thermal balance; curve (d) $D_{R,e}$ = 0.05 m, with wall thermal balance (wall thickness: 2 mm). Operating conditions: $y_{CH_4,0}$ = 1000 ppmV, $u_{G,0}$ = 0.1 m s^{-1}, t_c = 300 s (the profiles are taken in the middle of a semiperiod when the PSS is reached).

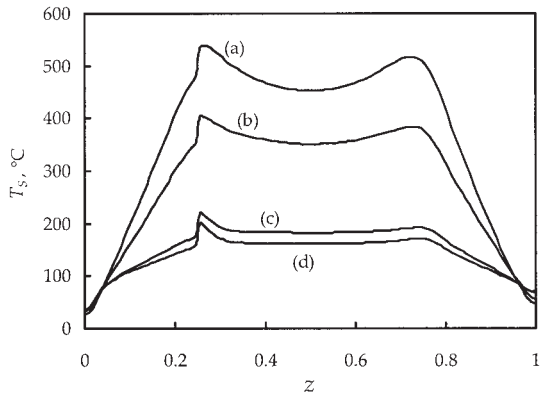

Figure 4. Comparison between the solid temperature profiles in a nonadiabatic reactor (h_W = 0.18 W m^{-2} K^{-1}) when the thermal balance of the wall is considered or not.

Operating conditions: $D_{R,e}$ = 0.05 m, $y_{CH_4,0}$ = 1000 ppmV, $u_{G,0}$ = 0.1 m s^{-1}, t_c = 300 s; wall thickness: 2 mm (the profiles are taken in the middle of a semiperiod when the PSS is reached). Curve (a): no wall; curve (b): quartz wall; curve (c) inconel wall; curve (d): inox wall.

the maximum solid temperature, which is a crucial parameter required to avoid catalyst deactivation, can be substantially different.

In a small-scale apparatus not only heat loss may affect the operation, but also the reactor wall, and in particular the heat conduction in the tube may play a significant role on the thermal balance of the system. Figure 3 shows a comparison between the solid temperature profiles calculated either taking or not taking into consideration the thermal balance of the reactor wall. It can be noticed that the effect is significant even if quartz material, which has a very low conductivity, is considered. Again, the effect of the wall is enhanced in the small-scale apparatus.

To reduce the heat conduction in the tube, two methods can be followed: (1) to decrease the tube thickness or (2) to adopt a less-conductive material. The former solution is easier, but it is not very efficient and, in addition, the tube thickness cannot be reduced below a certain value. The latter method, on the contrary, can be very efficient: a quartz tube should be used, given that its thermal conductivity is quite low and its resistance to high temperatures is excellent. Figure 4 shows a comparison between the solid temperature profiles obtained in the presence of different wall materials (whose properties are shown in Table 2). Thus, it can be concluded that the best materials to construct a bench-scale reactor—with the aim of decreasing the wall effect and approximating the adiabatic behavior—are those with low density, heat capacity, and thermal conductivity and with mechanical properties that allow for low thickness of the wall. Unfortunately, the materials that fit better with these requirements (Pyrex™, quartz, ceramic materials) are characterized by low mechanical strength and are prone to breaking. As a consequence, a stainless steel tube was considered, with a system devoted to compensating the heat losses.

The Bench-Scale Rig

The main innovative feature of the experimental setup is the temperature-control system that was designed to attain a dynamic compensation of the heat losses, preventing both overcompensation and bypassing of heat from the central part of the reactor to the ending sections. A perfect compensation is reached if the temperature of the reactor surroundings is equal to the temperature inside the reactor, at the same axial position, thus removing the driving force for heat transfer. A heating system with a PID (proportional–integral–derivative) controller was installed around the reactor: external temperature is the controlled parameter and the temperature inside the reactor is used as the set-point value. Because axial temperature profiles are not uniform and change with time as a result of unsteady-state operation, the heating system was divided into seven sections or band heaters, each of them independently controlled by different PID controllers. The central band heater is 0.10 m long and the others are 0.065 m long: this was the best compromise between efficiency and complexity of the device. To follow the dynamics of the temperature in the reactor, cooling air has to be supplied to cool down reactor surroundings when the bed temperature decreases, thus avoiding further heating that arises from the thermal inertia of the band heater.

Figure 5 shows a view from the top of one of the band heaters. Each of these bands is hinged, and therefore can be opened. In this figure number 1 corresponds to the entrance of air that acts as coolant. Such an entrance is constructed from a stainless steel tube welded to an external band support of the

Table 2. Main Physical Properties of the Wall Materials Considered

	Quartz	Inconel	Stainless Steel
ρ_W, kg m^{-3}	2200	8510	7800
$c_{p,W}$, J kg^{-1} K^{-1}	1037	450	510
λ_W, W m^{-1} K^{-1}	1.46	15.1	21.5

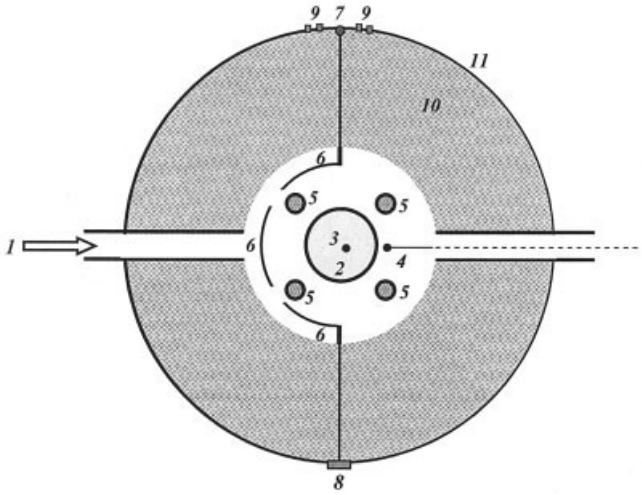

Figure 5. Band heater of the oven.

same material (11). The tube crosses an insulation layer (0.08 m thickness) of ceramic fiber (10). A K-type thermocouple (4) is inserted on a ceramic tube and crosses the external support and the insulation layer just above the coolant air outlet tube, thus measuring a temperature very close to the reactor wall (2). The thermocouple is located in the same axial position as that of the corresponding thermocouple inside the reactor (3). A deflector (6) avoids direct contact between the entering cooling air and the reactor wall, which may be the cause of nonuniform radial temperature profiles. The electric resistances (5) are located on cylindrically shaped longitudinal ceramic supports, anchored to both the upper and lower ceramic sheets limiting the modules. The four resistances are located between the external side of the reactor (2) and the internal side of the rock wool insulating layer (10). The electric connections (9) for these resistances are located in the back part of the external support at both sides of a hinge (7).

The entire temperature-control system is shown in Figure 6. The inner temperatures are measured by means of K-type thermocouples located in a sheath (1) inside the reactor (11). The signals of the thermocouples are sent to a Eurotherm 2500 modular PLC (6) that supports up to 16 modules; in this case, it contains six input modules (two input channels per module) working with voltage signals that are sent to a computer (3) by means of a RS232/RS485 converter (4). The computer is implemented with SCADA software for the control and data registration. Such computer receives the signals corresponding to the inner temperatures, registering and sending them as set-points to seven Eurotherm 2216 PID automatic controllers (6), one per module of the oven. The external temperature signals (2) taken by the controllers are sent directly to the converter and registered by the computer. These controllers execute the control action by means of solid-state relays (9) acting over the correspondent electric resistances (12). The demanded response for the controller is carried out by modulating the ratio of time "on" with respect to a complete cycle. The voltage applied to the resistances of each band heater can be fixed by means of a multichannel power regulator (10). From the computer, thanks to a two-channel relay output module on the PLC, it is also possible to act over the relays that run the gas preheating device (7) and switch the solenoid valves so as to carry out the flow reversals (8). This system is progressing through the patent application process.[13]

The reactor, made of 316 stainless steel, has an inner diameter and wall reactor thickness of dimensions 5.17×10^{-2} and 1.15×10^{-3} m, respectively. The length of the catalytic section is 0.246 m, whereas the two ending sections are filled with glass spheres 4×10^{-3} m in diameter. The catalyst is a γ-alumina—supported manganese oxide, shaped in spheres with a mean diameter of 4×10^{-3} m (BET surface area of 1.47×10^{3} m^2/kg and average pore diameter of 5.3×10^{-11} m). Kinetics of methane combustion over this catalyst was studied in an isothermal microreactor, which was previously used for other kinetic studies. The experimental apparatus and the methodology are described in detail in a previous paper.[14] A pseudo-first-order model proved to be accurate enough to describe the kinetics of methane combustion. Kinetic parameters and other operating conditions are detailed in Table 1.

The analysis of the gas streams was carried out by means of an HP 6890 GC equipped with a HP-5 capillary column and flame ionization detector (FID).

Results of the Experimental Tests

Experiments without chemical reaction can be used to provide initial insight into the thermal behavior of the reactor and to compare it with that of an adiabatic device. This kind of experiments was also suggested by other authors, such as van de Beld et al.,[15] for example, who performed a preheating experiment for verifying the adiabatic behavior of their device. In the case of our experimental equipment, preheating tests consisted in turning on the electric preheater and, after it reaches a constant temperature, starting to feed an air stream to the reactor. Then, the temperature profile in the bed is registered until a steady state is obtained. The temperature of the electric preheater during the experiment was about 540°C, leading to a final steady temperature in the bed of about 400°C. Figure 7 (top graph) shows that the steady-state axial temperature profile obtained in the reactor was almost flat, as expected in an adiabatic system. Also, the temperatures measured in the central axial position of each band heater are very close to those predicted by the model for adiabatic operation. Moreover, Figure 7 (bottom graph) shows that the dynamic evolution of the temperature is also close to model predictions for adiabatic operation; in this figure, such evolution is shown for the center of the bed as an example of the results obtained in the reactor.

A second preliminary experiment without chemical reaction was performed. It consisted in cooling down the bed, operating with flow reversal, and feeding air at room temperature to the reactor. In this experiment, once the reactor is totally preheated, the electric preheater is turned off. Figure 8 shows the evolution of the temperature in the axial positions corresponding to the second (from the top), fourth, and sixth module as an example of the good agreement between experiments and simulations (where, as usual, adiabatic operation is assumed).

Once the adiabatic behavior without chemical reaction was stated, further experiments were carried out with chemical reaction (methane catalytic combustion). In each experiment the procedure is the same used in the cooling down experiment

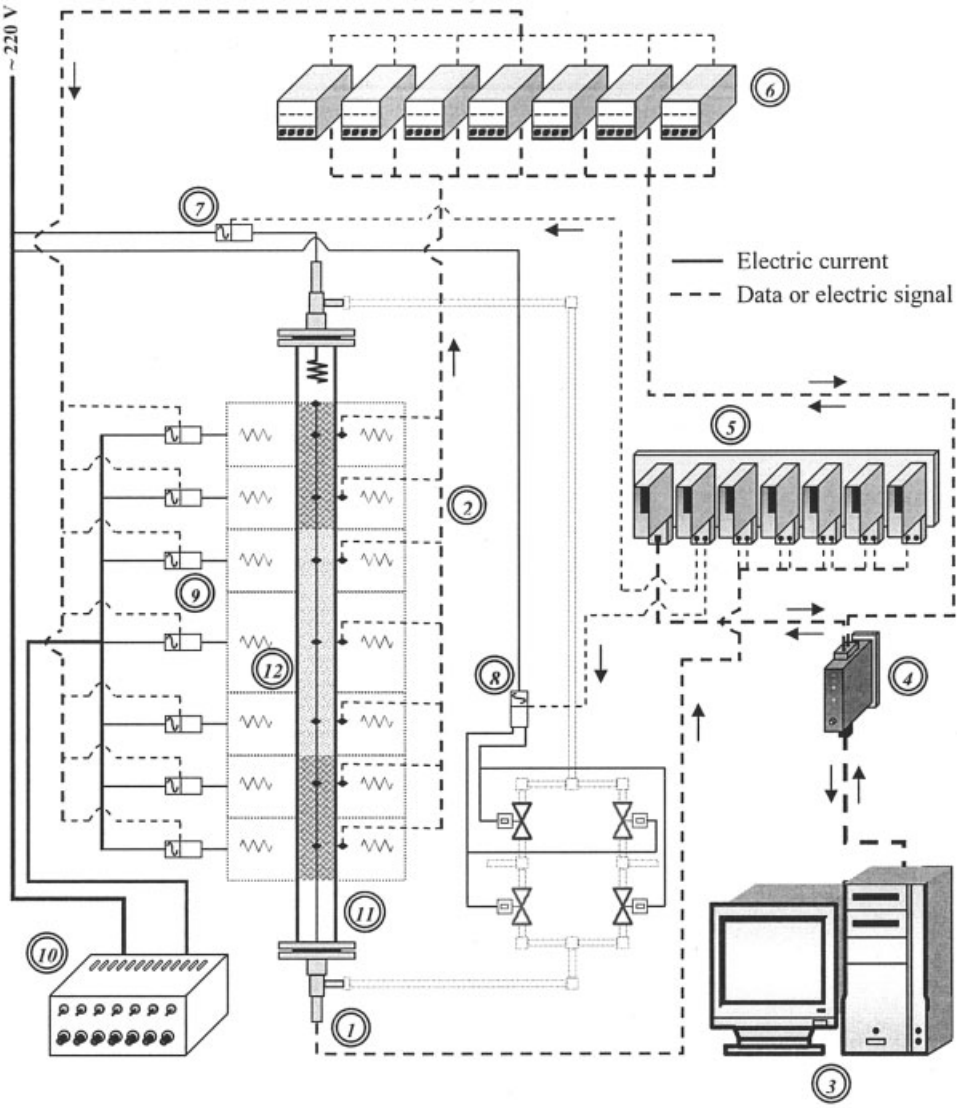

Figure 6. Overall view of the temperature control system of the reactor.

previously described, but changing the pure air stream by a lean methane–air mixture (3500–4500 ppmV methane in air). Several experiments were carried out, changing the values of the main operating parameters, that is switching time, inlet concentration, and surface gas velocity. The range of values used for each of the variables was chosen according to the operation limits of the experimental rig.

Figure 9 shows the dynamic evolutions of the temperature in the center of the reactor and in the two ending inert sections when the combustion of methane (3500 ppmV) in air takes place; the experimental values are compared to those obtained by simulation of the adiabatic reactor, also proving that under these conditions the dynamic compensation of the heat losses is effective in attaining adiabatic operation, avoiding overcompensation. It can also be noticed that the best agreement between experimental results and simulations of the adiabatic system (which is the benchmark of the analysis) is obtained in the central position, which is a general trend throughout the work. This is a consequence of the fact that poor oscillations of the temperature occur in this part; moreover, the temperature profile in the central area is almost flat, thus avoiding problems arising from slight deviations from the thermocouple axial positions supposed in the simulations and the actual positions, which may be responsible for the deviations observed in the other sections.

Figure 10 shows the simulated axial temperature profiles and the actual measurements for three different instants after the PSS was reached: the beginning, the middle, and the end of a cycle. These results confirm that the behavior is very close to adiabatic behavior, as well as the accuracy attained in determination of the model parameters. This conclusion is based not only on the good agreement between experimental measurements and simulated profiles, but also on the absence of local temperature minima in the central zone of the axial profiles, which are caused by the existence of a nonnegligible heat flux between the reactor and its surroundings, as reported by van de

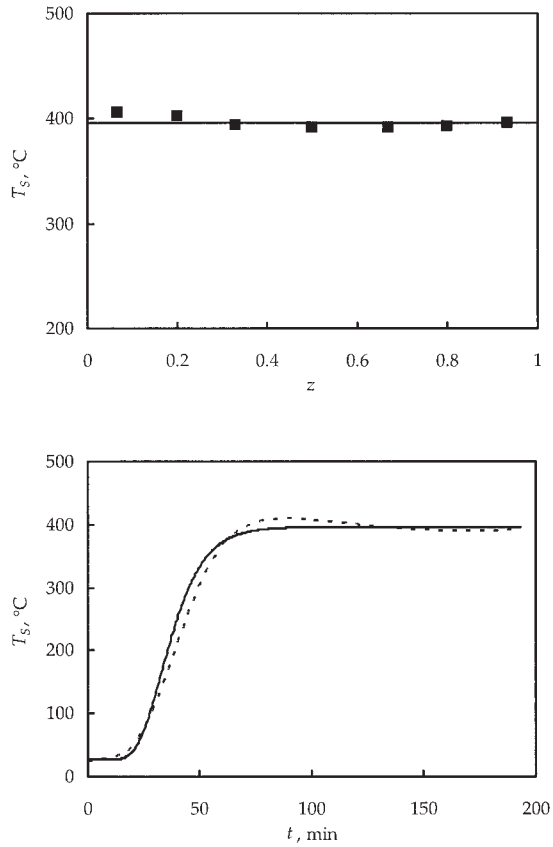

Figure 7. Experimental (symbols) and simulated (solid lines) steady-state axial temperature profile for a preheating experiment (top graph) and comparison between the measured (dotted line) and the simulated values (solid line) of the solid temperature in the central part of the reactor (bottom graph).

$u_{G,0} = 0.155$ m s^{-1}.

Beld et al.[15] and Cunill et al.[5] Similarly, axial temperature profiles do not present local maxima near the inert-catalyst boundary surface. This last effect would reveal an underuse of the treatment capacity of the reactor because it indicates that the reaction occurs just at the ends of the active section of the bed.[16]

Influence of the Main Operating Conditions

Switching time, inlet concentration, and inlet flow rate (and thus gas surface velocity) emerge as the most important operating variables in the catalytic combustion of hydrocarbons in the RFR. In this work, experiments involving the variation of these three parameters were carried out, with the aim of highlighting the effect of these variables on the reactor performance and testing the effectiveness of the temperature-control system designed over a wide range of operating conditions. The analysis is carried out taking into consideration various parameters, but only the maximum solid temperature, evaluated among the seven measured values, is shown in Figure 11. Maximum temperature is chosen because it is the best indicator of the reactor performance, allowing us to distinguish between an extinguished or an ignited reactor, and also allowing to know whether the temperature is within the safety limits for the most thermal sensible parts of the treatment unit, typically the catalyst.

In the middle chart of Figure 11, a very slight influence of switching time is observed on the solid maximum temperature and the model accurately predicts this behavior. The absence of noticeable dependency of the maximum temperature with the switching time within certain intervals of the latter was already noticed in a previous work[17]: noticeable changes in the maximum solid temperature were found (1) just at very low switching times, where the maximum temperature quickly increases when approaching zero; and (2) at high values of the switching time, where maximum temperature quickly decreases when approaching the maximum switching time that allows for autothermal behavior.

With respect to the surface velocity, the experimental values are still in good agreement with the simulations of the adiabatic reactor, although in this case the degree of dependency of the

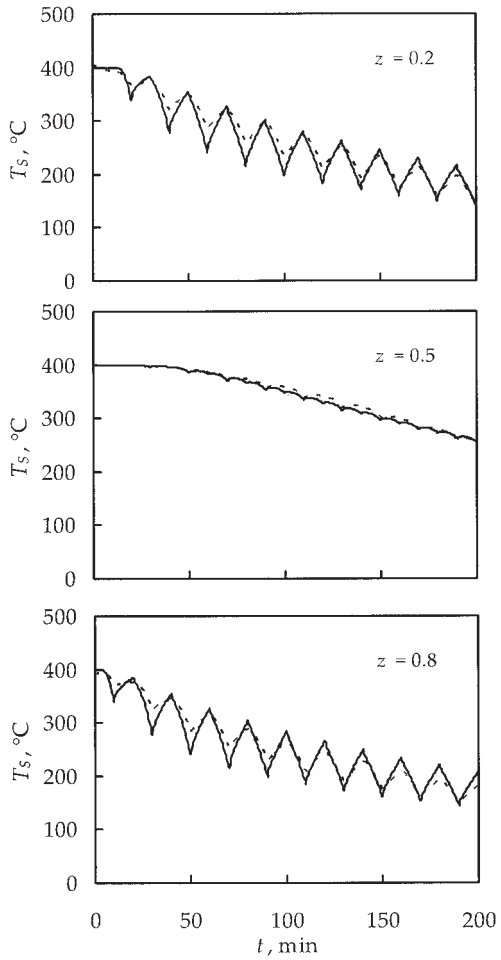

Figure 8. Experimental (dotted lines) and simulated (solid lines) evolution of the solid-phase temperature in a reverse-flow experiment without chemical reaction for different axial positions.

$u_{G,0} = 0.155$ m s^{-1}, $t_c = 600$ s.

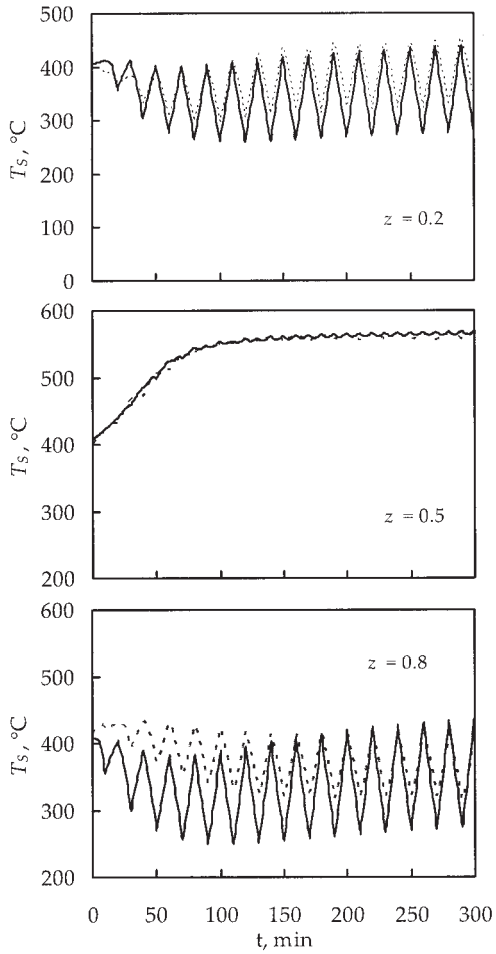

Figure 9. Experimental (dotted lines) and simulated (solid lines) evolution of the solid-phase temperature in a reverse-flow experiment with chemical reaction for different axial positions.

$u_{G,0}$ = 0.143 m s^{-1}, $y_{CH_{4,0}}$ = 3500 ppmV, t_c = 600 s.

maximum temperature on this parameter is vitally important, in that it is observed that the maximum temperature increases with gas velocity, the effect of which is more pronounced at lower surface velocities. This behavior is typical of systems involving phenomena that lead to opposite effects. In this case an increase of the surface velocity implies an increase of the heat generated by the reaction, but it also implies an increase of the convective heat transmission, thus contributing to a decrease in the maximum temperature in the reactor. Depending on the surface velocity considered, the former or the latter effect prevails. This behavior was previously found by van de Beld et al.[15] and Sapundzhiev et al.[18] Stable operation is not possible for both very low and very high values of the surface velocity, explained as follows: in the former case the heat generation rate is too low to maintain the ignition of the reactor and in the latter case the heat dispersion and the creeping velocity of the hot front are so high that they do not allow temperatures high enough within the limits of the bed.

The dependency of the maximum solid temperature on the methane concentration fed to the reactor, as shown in Figure 11 (bottom chart), is observed to be almost linear. These results are consistent with previous literature results.[19]

Conclusions

An innovative system was designed and tested for the purpose of compensating heat losses in bench-scale reactors, working in unsteady-state conditions, and proved to be effective in achieving results similar to those obtained in adiabatic conditions. This allows for a correct scale-up of the results obtained in bench-scale apparatus to industrial-size reactors.

A detailed model was considered to simulate the behavior of the system, taking into consideration the influence of the wall reactor, which was demonstrated to strongly influence the thermal stability of the system in a bench-scale apparatus. Modeling results were compared to values obtained in a bench-scale rig, showing the effectiveness of the heat compensation system under a wide range of operating conditions.

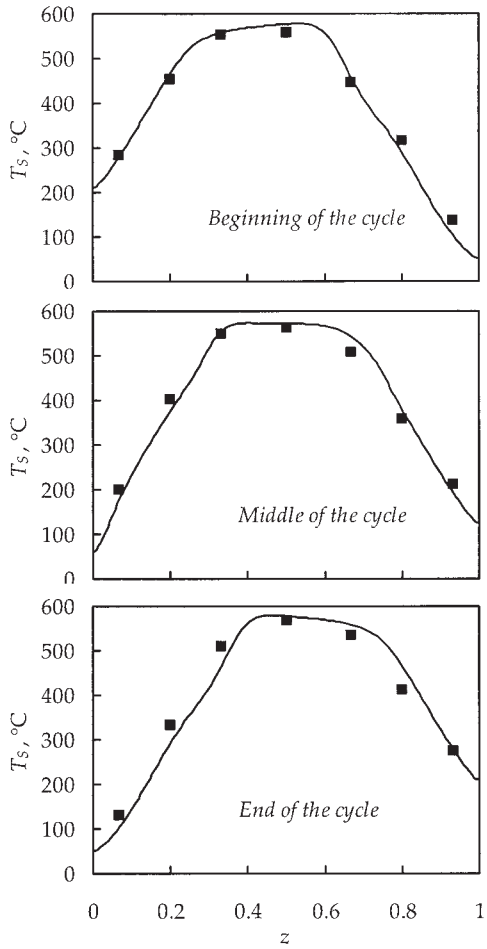

Figure 10. Simulated (solid line) axial temperature profiles and actual measurements (symbols) for different time instants of a cycle, when the PSS was reached.

$u_{G,0}$ = 0.143 m s^{-1}, $y_{CH_{4,0}}$ = 3500 ppmV, t_c = 600 s.

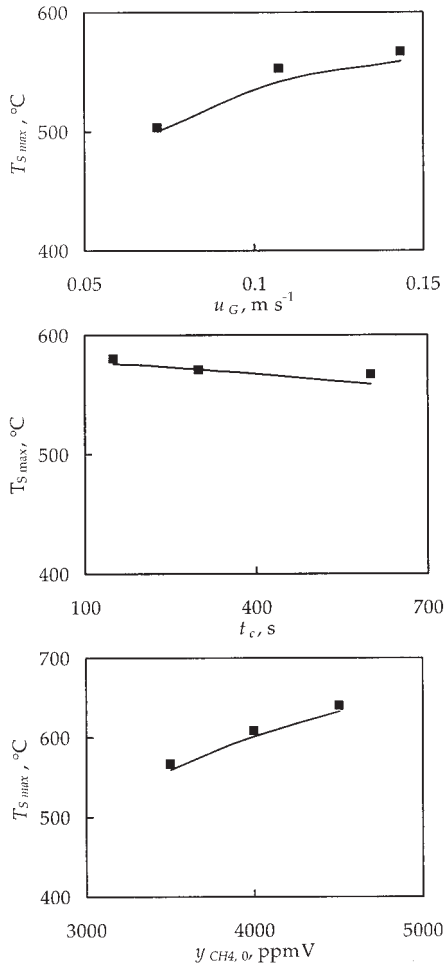

Figure 11. Influence of the switching time (middle graph: $u_{G,0} = 0.143$ m s^{-1}, $y_{CH_{4,0}} = 3500$ ppmV), of the gas velocity (top graph: $y_{CH_{4,0}} = 3500$ ppmV, $t_c = 600$ s), and of the inlet methane concentration (bottom graph: $u_{G,0} = 0.143$ m s^{-1}, $t_c = 600$ s) on the reactor maximum temperature.

Comparison between experimental (symbols) and simulated (solid lines) values.

Acknowledgments

This work was financially supported by the European Community (Contract ENV4-CT97-0599). Financial support of Italian and Spanish Ministries of University and Research (Project "Integrated Actions Italy–Spain") and contributions of M. Cittadini and M. Vanni to initial design of the apparatus are also gratefully acknowledged.

Notation

a_v = external particle surface area per unit volume of reactor, m^{-1}
c = molar concentration, mol m^{-3}
c_p = specific heat at constant pressure, J kg^{-1} K^{-1}
D_{eff} = effective mass dispersion coefficient, m^2 s^{-1}
d_P = pellet diameter, m
D_R = reactor diameter, m
E_a = activation energy, J kmol^{-1}
ΔH_f = molar enthalpy of formation, J mol^{-1}
h = gas–solid heat transfer coefficient, J m^{-2} K^{-1} s^{-1}
k_∞ = pre-exponential factor, s^{-1}
k'_∞ = frequency factor, mol kg^{-1} s^{-1} Pa^{-1}
k_{eff} = effective heat dispersion coefficient, J m^{-1} K^{-1} s^{-1}
k_G = gas–solid mass transfer coefficient, mol m^{-2} s^{-1}
k_r = kinetic constant, s^{-1}
L = total reactor length, m
N_R = number of reactions
n_r = number of components in the mixture
Pr = Prandtl number
R = ideal gas constant, J K^{-1} mol^{-1}
R' = reaction rate, s^{-1}
Re_P = particle Reynolds number
Sc = Schmidt number
T = temperature, K
t = time, s
t_c = switching time, s
u = surface velocity, m s^{-1}
v = interstitial velocity, m s^{-1}
x = axial reactor coordinate, m
y = molar fraction
z = nondimensional axial reactor coordinate, $z = x/L$

Greek letters

ε = bed void fraction
η = effectiveness factor
λ = thermal conductivity, J m^{-1} K^{-1} s^{-1}
ν = stoichiometric coefficient
ρ = density (or apparent density for the solid), kg m^{-3}

Subscripts and superscripts

e = external value
G = gas phase
i = internal value
max = maximum value
S = solid phase or solid surface
W = reactor wall

Abbreviations

PSS = periodic steady state
RFR = reverse-flow reactor

Literature Cited

1. Matros YS, Bunimovich GA. Reverse-flow operation in catalytic reactors. *Catal Rev Sci Eng*. 1996;38:1-68.
2. Fissore D, Barresi AA. On the influence of the catalyst physical properties on the stability of forced unsteady-state after-burners. *Chem Eng Res Des Trans IChemE A*. 2003;81:611-617.
3. Van de Beld L, Westerterp KR. Air purification in a reverse-flow reactor: Model simulations vs. experiments. *AIChE J*. 1996;42:1139-1148.
4. Purwono S, Budman H, Hudgins RR, Silveston PL, Matros YS. Runaway in packed bed reactors operating with periodic flow reversal. *Chem Eng Sci*. 1994;49:5473-5487.
5. Cunill F, Van de Beld L, Westerterp KR. Catalytic combustion of very lean mixtures in a reverse flow reactor using an internal electrical heater. *Ind Eng Chem Res*. 1997;36:4198-4206.
6. Nieken U, Kolios G, Eigenberger GA. Fixed-bed reactors with periodic flow reversal: Experimental results for catalytic combustion. *Catal Today*. 1994;20:335-350.
7. Eigenberger G, Nieken U. Catalytic combustion with periodical flow reversal. *Chem Eng Sci*. 1988;43:2109-2119.
8. Zufle H, Turek T. Catalytic combustion in a reactor with periodic flow reversal: 1. Experimental results. *Chem Eng Process*. 1997;36:327-340.
9. Van de Beld L. *Air Purification by Catalytic Oxidation in an Adiabatic Packed Bed Reactor with Periodic Flow Reversal*. PhD Thesis, University of Twente, Enschede, The Netherlands; 1995.
10. Dixon A, Cresswell DL. Theoretical prediction of effective heat transfer parameters in packed beds. *AIChE J*. 1979;25:663-676.
11. Edwards MF, Richardson JF. Gas dispersion in packed beds. *Chem Eng Sci*. 1968;23:109-123.

12. Hindmarsh AC. ODEPACK, a systematized collection of ODE solvers. In: Stepleman RS et al., eds. *IMACS Transactions on Scientific Computation*. Vol. 1. Amsterdam: North-Holland; 1983.
13. Díez F, Vega A, Ordóñez S, Hevia MAG, Fissore D, Cittadini M, Vanni M, Barresi A, Baldi G. *Dispositivo para el control de flujo de calor a través de la pared en equipos pequeños*. Spanish Patent Appl. No. P200400625; 2004.
14. Hurtado P, Ordóñez S, Díez FV, Sastre H. Development of a kinetic model for the oxidation of methane over Pd/Al_2O_3 at dry and wet conditions. *Appl Catal B*. 2004;51:229-238.
15. Van de Beld L, Borman RA, Deckx OR, Woezik BAA, Westerterp KR. Removal of volatile organic compounds from polluted air in a reverse flow reactor: An experimental study. *Ind Eng Chem Res*. 1994;33:2946-2956.
16. Salomons S, Hayes RE, Poirier M, Sapoundjiev H. Flow reversal reactor for the catalytic combustion of lean methane mixtures. *Catal Today*. 2003;83:59-69.
17. Hevia MAG, Fissore D, Ordóñez S, Díez FV. Catalytic combustion of methane lean mixtures. In: Macías-Machín A, Umbría J, eds. *Chemical Industry and Environment IV*. Vol. 2. Universidad de Las Palmas de Gran Canaria: EMA; 2003:175-183.
18. Sapundzhiev C, Chaouki J, Guy C, Klvana D. Catalytic combustion of natural gas in a fixed bed reactor with flow reversal. *Chem Eng Commun*. 1993;125:171-186.
19. Ben-Tullilah M, Alajem E, Sheintuch M. Flow-rate effects in flow reversal reactors: Experiments, simulations approximations. *Chem Eng Sci*. 2003;58:1135-1146.

Manuscript received July 23, 2004, and revision received Oct. 24, 2004.